Electronic Supplementary Material (ESI) for Journal of Materials Chemistry C.

Supporting Information

Ultrapure blue organic light-emitting diodes exhibiting 13-nm full width at half-maximum

Tiangeng Liu,[a] *Cong Cheng,*[a] *Weiwei Lou,* [b] *Chao Deng,**[a] *Junyuan Liu,*[a] *Dan Wang,*[a] *Taiju Tsuboi,*[a] *Qisheng Zhang**[ac]

[a] MOE Key Laboratory of Macromolecular Synthesis and Functionalization, Department of Polymer Science and Engineering, Zhejiang University, Hangzhou 310027, China.
[b] Zhejiang Hongwu Technology Co., Ltd., Taizhou 317100, China.
[c] State Key laboratory of Clean Energy Utilization, Zhejiang University, Hangzhou 310027, China.
E-mail: qishengzhang@zju.edu.cn; 0016831@zju.edu.cn

Contents

1. Supplemental Tables and Figures

Table S1. Absorption maximum ($\lambda_{abs,max}$), emission maximum ($\lambda_{em,max}$), PLQY (Φ), fluorescence lifetime (τ), and fluorescence rate (k_F) of the investigated compounds in toluene at room temperature (RT).

Compounds	$\lambda_{abs,max}$ (nm)	$\lambda_{em,max}$ (nm)	FWHM (nm)	Φ	τ (ns)	k_F ($\times 10^8$ s^{-1})
DICz	443	446	10	0.99	5.5	1.8
mtPh$_2$DICz	450	457	13	0.99	4.3	2.3
mMes$_2$DICz	443	445	10	0.99	5.1	2.0

Table S2. Emission maximum ($\lambda_{em,max}$), PLQY (Φ), and fluorescence lifetime (τ) of the investigated compounds in mCP films at room temperature (RT).

	concentration	$\lambda_{em,max}$ (nm)	FWHM (nm)	Φ	τ (ns) [a]
DICz	1 wt.%	451	54	0.93	1.53
	2 wt.%	465	53	0.53	1.51
	4 wt.%	474	55	0.35	0.70
mtPh$_2$DICz	1 wt.%	461	51	0.94	1.26
	2 wt.%	467	55	0.92	1.21
	4 wt.%	483	59	0.89	0.85
mMes$_2$DICz	1 wt.%	451	16	0.99	5.04
	2 wt.%	454	46	0.79	2.31
	4 wt.%	455	49	0.53	1.51

[a] Determined from the time the fluorescence intensity decays to 1/e of the initial value.

Table S3. The comparison of device data of mMes$_2$DICz doped devices and deep blue OLED devices reported in the literatures to date.

Type	Emitters	$\lambda_{EL,max}$ (nm)	FWHM (nm)	CIE	EQE$_{max}$ (%)	EQE$_{1000}$ (%)	Ref.
TADF	tPBisICZ	452	21	(0.15,0.05)	23.1	N/A	1

Flu.	t-IDIDCz	401	14	(0.16,0.02)	3.3	N/A	2
Flu.	m-FLDID	407−411	17−27	(0.17, 0.02)	4.4−5.2	N/A	3
Flu.	M1	420	~50	(0.17, 0.05)	2.0	N/A	4
Flu.	M2	428	~50	(0.17, 0.06)	3.0	N/A	
Flu.	HAMT2SO2	416	53	(0.16, 0.06)	2.2	N/A	5
Flu.	TPA–PIM	420	35	(0.16, 0.05)	3.2	~3	6
Flu.	TPDAAn	435	46	(0.15, 0.05)	2.7	N/A	7
Flu.	TPDAPhAn	435	46	(0.15, 0.06)	3.7	N/A	
Flu.	dTPDDAn	435	51	(0.16, 0.06)	4.0	N/A	
HLCT	DPM	428	52	(0.16,0.05)	4.0	N/A	8
HLCT	TDPM	424	49	(0.16,0.05)	2.6	N/A	
HLCT	SAFpCN	432	50	(0.15, 0.05)	4.6	3.3	9
HLCT	SAFmCN	413	56	(0.16, 0.05)	3.2	N/A	
HLCT	DSiTPI	396	48	(0.16,0.05)	7.4	5.0	10
HLCT	CSiTPI	388	47	(0.16,0.05)	5.2	4.3	
Flu.	mMes$_2$DICz	450	13	(0.15,0.04)	9.5	9.2	This work

Table S4. Emission maximum (λ_{max}), turn-on voltage (V_{on}), full width at half-maximum (FWHM), external quantum efficiency maximum (EQE$_{max}$), external quantum efficiency at 100 mA/cm^2 (EQE$_{100}$), luminance maximum (L_{max}), and Commission Internationale de L'Eclairage (CIE) Coordinates of the OLEDs with different emitters.

Emitter	Doping concentration	λ_{max} (nm)	V_{on} (V)	FWHM (nm)	EQE$_{max}$ (%)	EQE$_{100}$ (%)	L_{max} (cd/m^2)	CIE
DICz	1 wt.%	449	3.8	35	5.5	4.6	9146	(0.14, 0.10)
mtPh$_2$DICz	1 wt.%	453	3.4	33	10.3	8.3	20485	(0.13, 0.14)
mMes$_2$DICz	1 wt.%	450	3.3	13	9.5	7.8	7780	(0.15, 0.04)
mMes$_2$DICz	2 wt.%	451	3.1	15	10.2	8.2	10307	(0.14, 0.05)
mMes$_2$DICz	4 wt.%	452	3.0	33	10.6	8.6	13594	(0.14, 0.09)
t-DABNA	1 wt.%	462	3.2	23	9.6	7.7	11373	(0.13, 0.07)
tBu$_4$pICz	1 wt.%	444	3.4	27	6.8	5.1	4813	(0.15, 0.04)

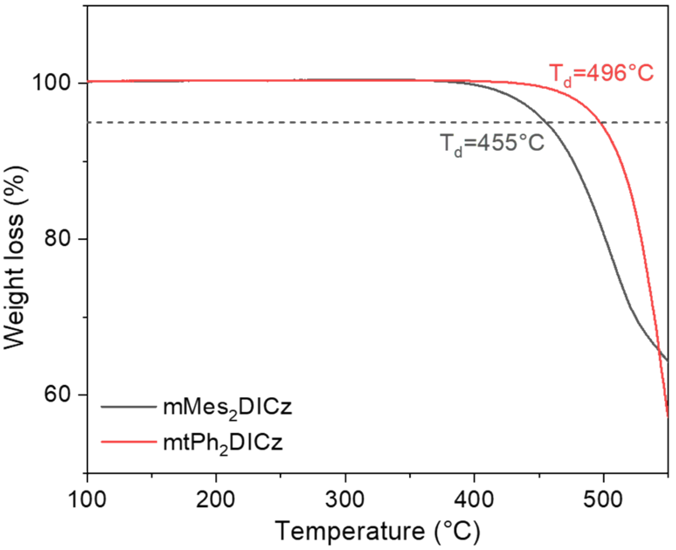

Figure S1. TGA curves of the emitters under nitrogen flow.

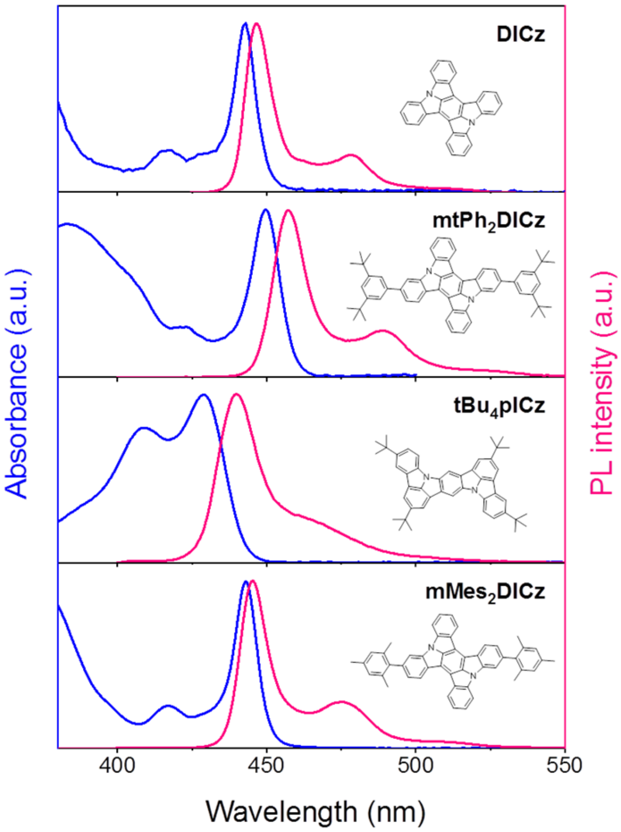

Figure S2. The absorption and emission spectra of DICz, mtPh$_2$DICz, tBu$_4$pICz and mMes2DICz in toluene (10^{-6} M).

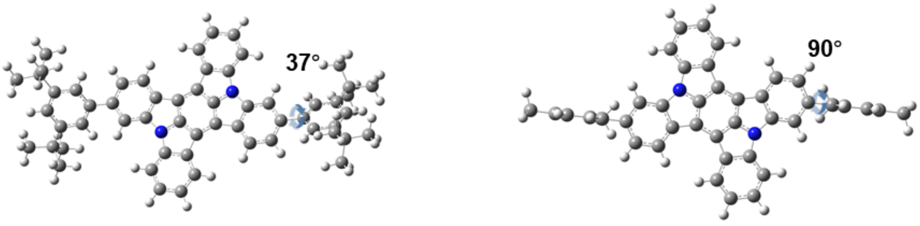

$mtPh_2DICz$ **$mMes_2DICz$**

Figure S3. Geometries of $mtPh_2DICz$ and $mMes_2DICz$ in their ground state optimized by DFT calculations at the B3LYP/6-31G* level.

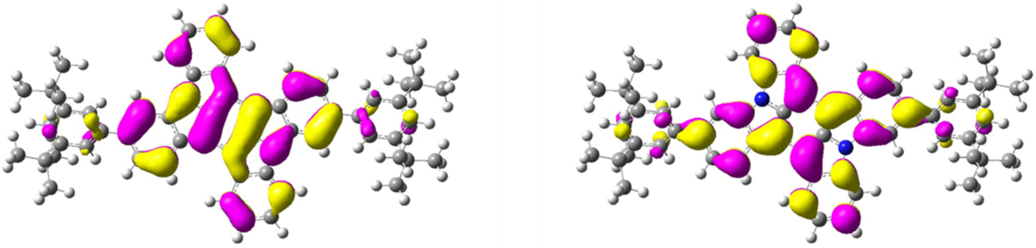

HOMO **LUMO**

Figure S4. HOMO and LUMO distribution of $mtPh_2DICz$ in the ground state.

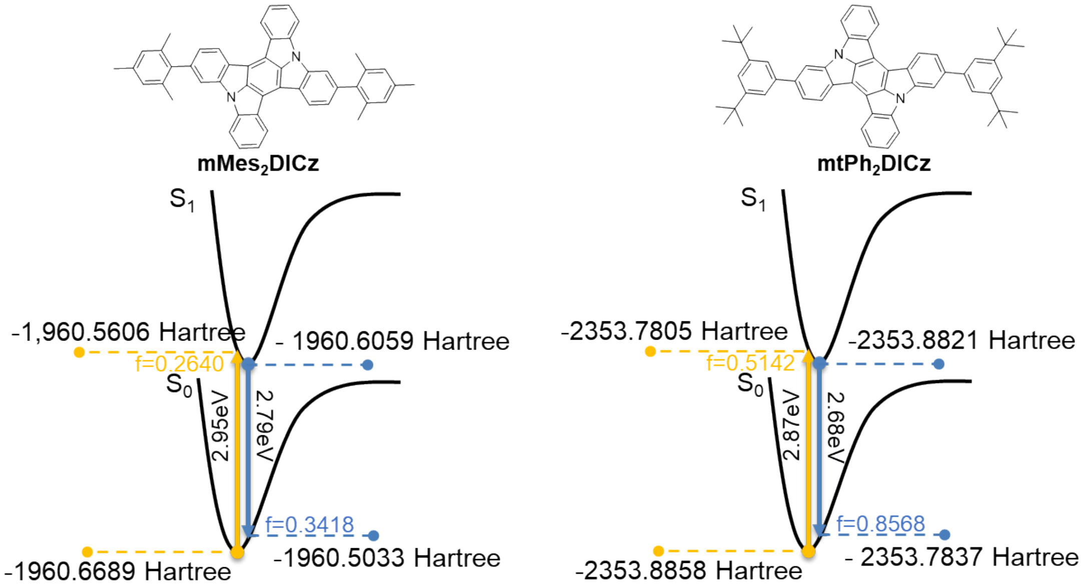

Figure S5. The potential energy surfaces for ground and excited states as well as the energy calculated at B3LYP-D3BJ/6-31G(d,p) level for $mMes_2DICz$ and $mtPh_2DICz$ in toluene.

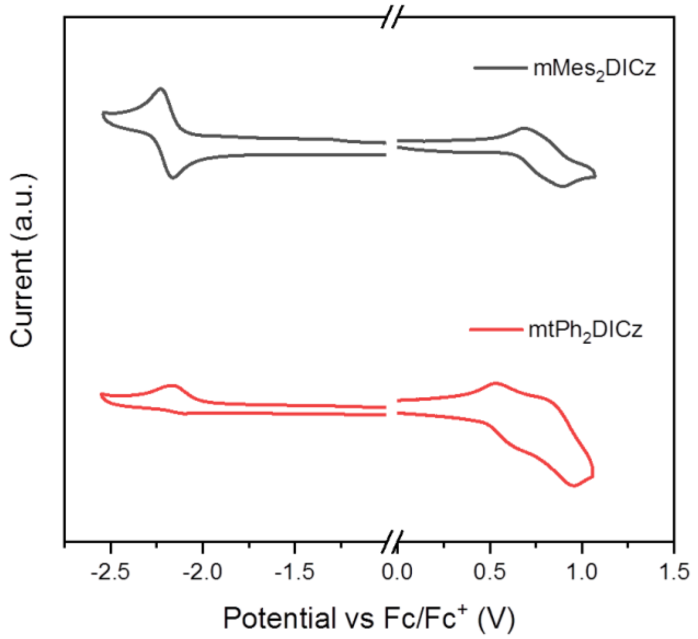

Figure S6. Cyclic voltammograms of mMes$_2$DICz and mtPh$_2$DICz in DCM (oxidation) and DMF (reduction). The LUMO and HOMO energy levels were calculated to be -5.45 eV and -2.69 eV for mMes$_2$DICz, respectively, and -5.28 eV and -2.77 eV, respectively, from the reduction and oxidation curves following the formula: HOMO = $-[E_{ox}-E(\mathrm{Fc/Fc^+}) + 4.8]$ eV and LUMO = $-[E_{re} - E(\mathrm{Fc/Fc^+}) + 4.8]$ eV, respectively.

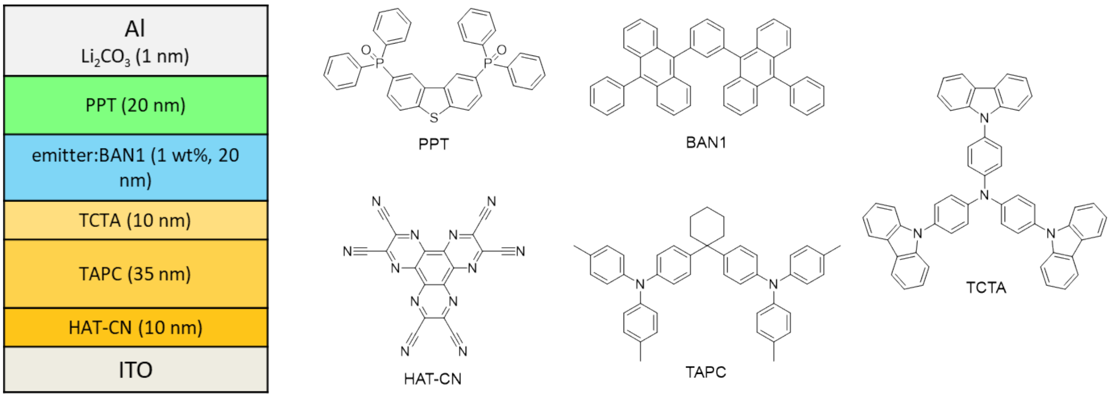

Figure S7. Structure of OLED devices and the compounds used in them.

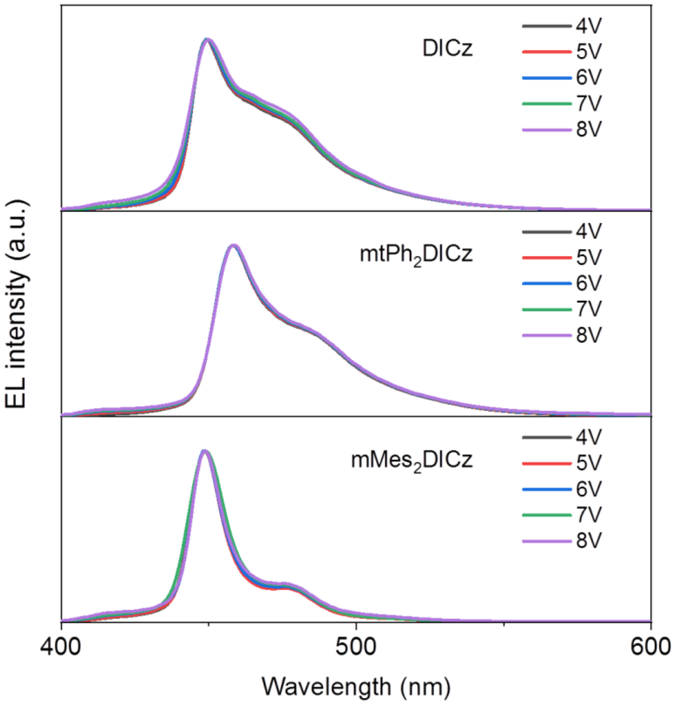

Figure S8. Voltage-dependent electroluminescent spectra for the devices based on DICz (a), mtPh$_2$DICz (b) and mMes$_2$DICz(c).

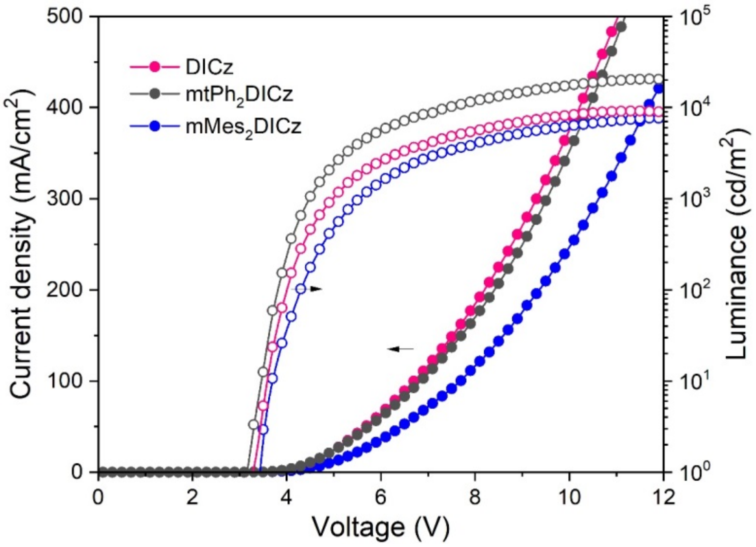

Figure S9. Current density–voltage–luminance characteristics of OLEDs containing the investigated compounds. The doping concentration of the emitter in emitting layer is 1 wt.%.

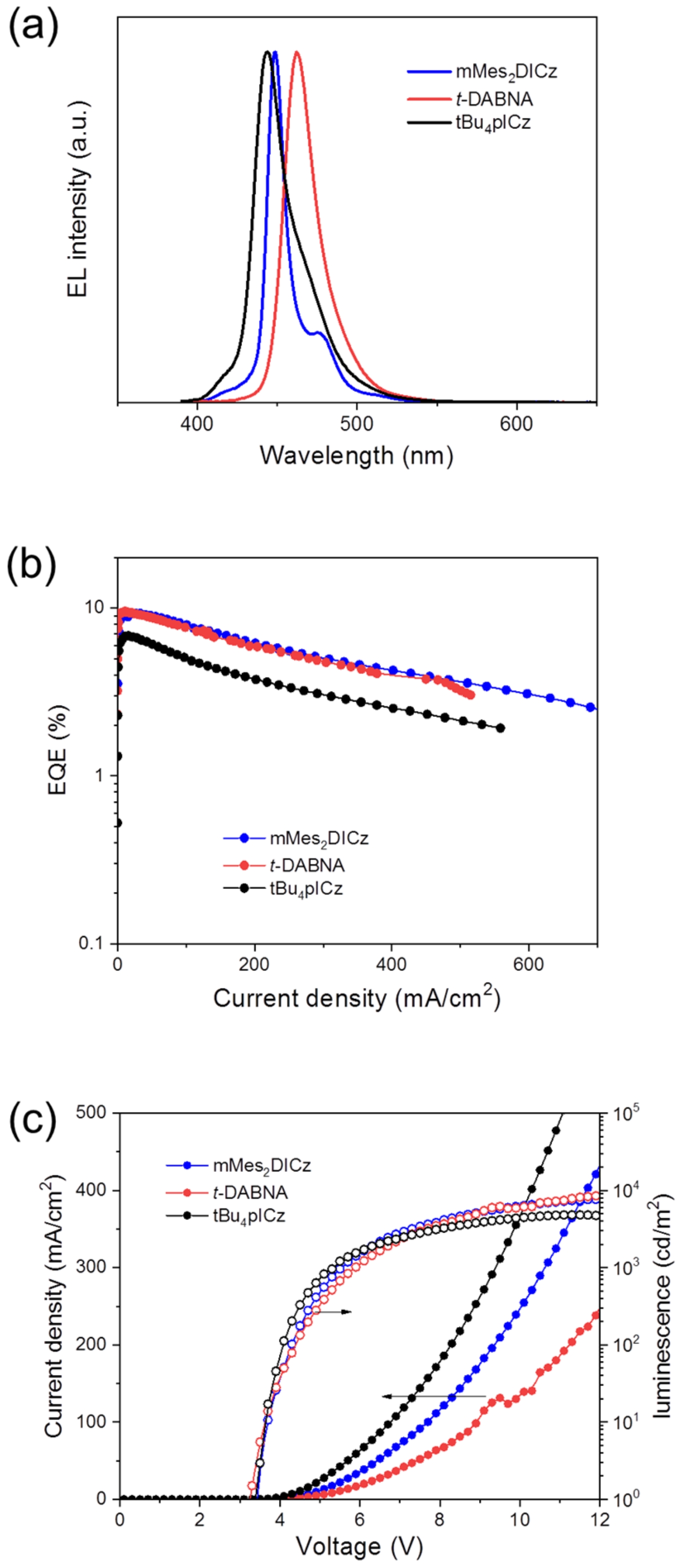

Figure S10. Performance of the mMes$_2$DICz-, *t*-DABNA- and tBu$_4$pICz-based OLEDs: a) Electroluminescence spectra at 10 mA/cm^2; b) EQE−current density characteristics; c) Luminance−current density−voltage characteristics.

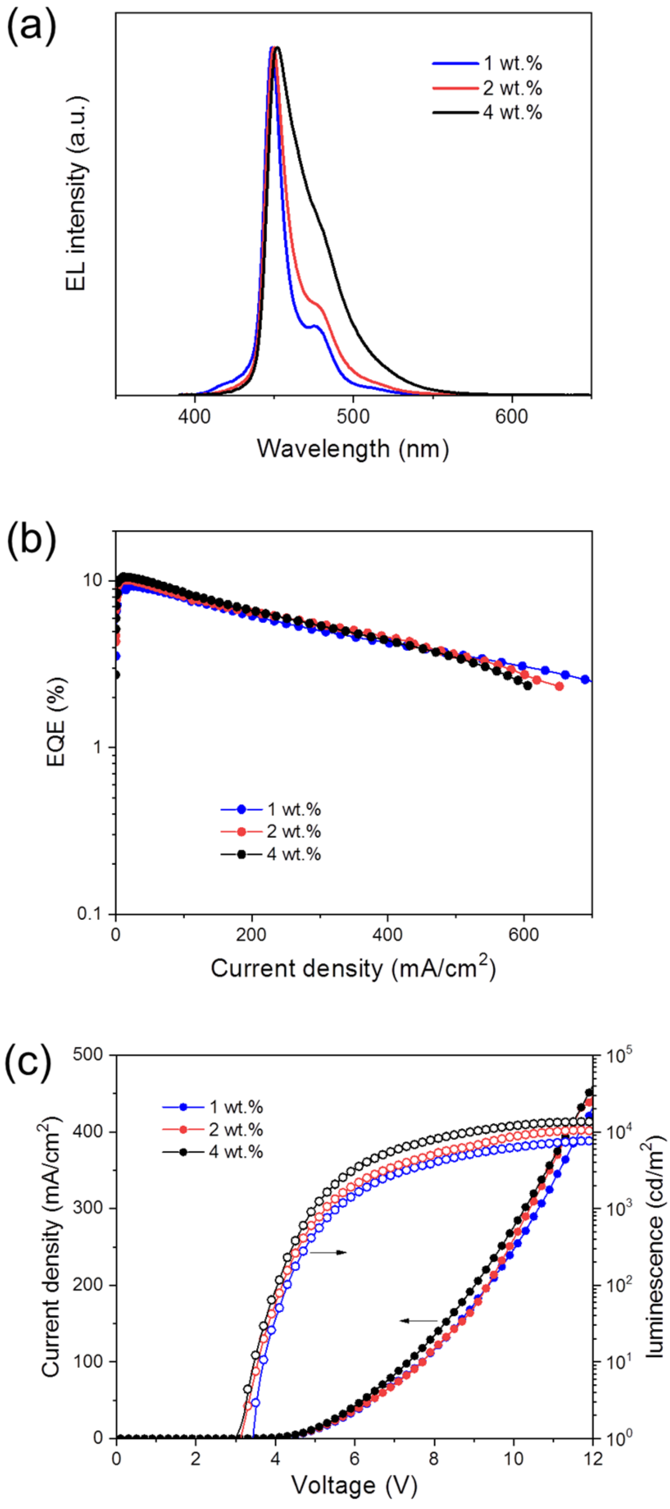

Figure S11. Performance of the $mMes_2DICz$-based OLEDs: a) Electroluminescence spectra at 10 mA/cm^2; b) EQE−current density characteristics; c) Luminance−current density−voltage characteristics.

2. Experimental Section

2.1 Materials and measurement:

All solvents and starting materials were purchased from commercial resources and were used as received. OLED materials for device fabrication were purchased from Jilin optical and electronic materials Co. Ltd and were used as received. Nuclear magnetic resonance spectroscopy (NMR) were recorded on a Bruker Avance III 400 spectrometer (^{1}H: 400 MHz and ^{13}C: 101 MHz) or Brulcer Co. DMX-500 spectrometer (^{1}H: 500 MHz and ^{13}C: 126 MHz) at room temperature (RT) using $CDCl_3$ as solvent and tetramethylsilane (TMS) as internal reference. Mass spectra were recorded by Bruker UltraFLEX MALDI-ToF mass spectrometer in the reflector mode. Elemental analyses (C, H, N) were carried out with a Vario MICRO cube (Elementar).

2.2 Synthesis:

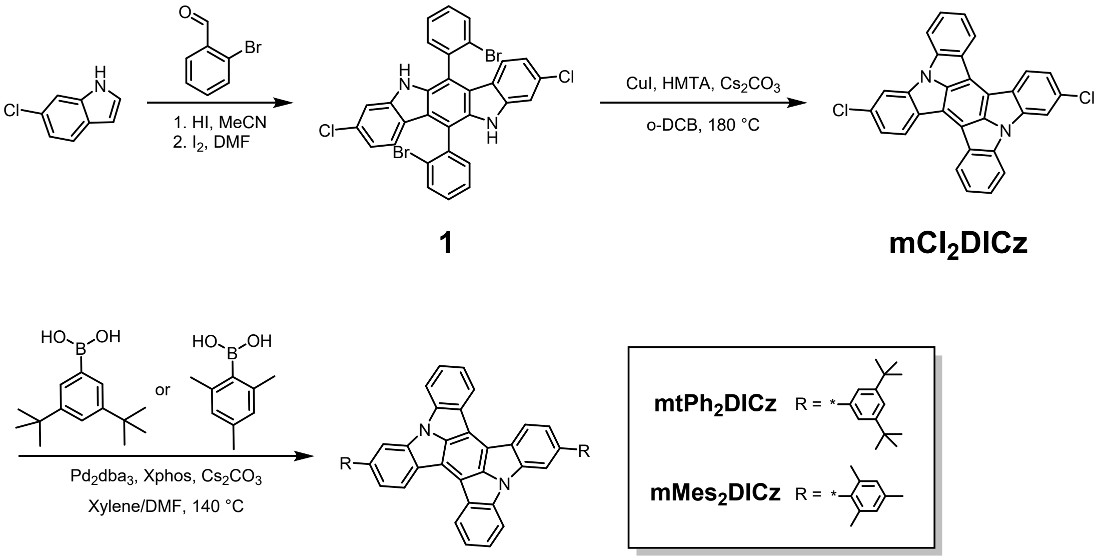

Scheme S1. Synthetic procedure of $mtPh_2DICz$ and $mMes_2DICz$.

6,12-Bis(2-bromophenyl)-3,9-dichloro-5,11-dihydroindolo[3,2-b]carbazole (1)

2-Bromobenzaldehyde (11.10 g, 60 mmol), 6-Chloroindole (9.10 g, 60 mmol) were sequentially added to the 120 mL acetonitrile in a 250 mL round flask. Then 4mL HI (45%) was added to the flask. The mixture was refluxed overnight. After cooling to

RT, white solid precipitate was collected by filtration. This white solid was added to a 250 mL round flask with 120 mL DMF. Then I_2 (30.46 g, 120 mmol) was added. The solution was refluxed 4 h. After cooling to RT, the mixture was poured into saturated $Na_2S_2O_3$ solution (200 mL) and stirred for another 1h. **1** was collected by filtration without further purification (9.23 g, 48.4%). ^{1}H NMR (400 MHz, Chloroform-*d*) δ 7.96 (dd, *J* = 7.8, 0.9 Hz, 2H), 7.79 (s, 2H), 7.64 – 7.59 (m, 4H), 7.53 (ddd, *J* = 7.9, 5.4, 3.8 Hz, 2H), 7.34 (d, *J* = 1.2 Hz, 2H), 6.93 (d, *J* = 1.2 Hz, 4H).

3,12-Dichlorodibenzo[2,3:5,6]pyrrolizino[1,7-bc]indolo[1,2,3-lm]carbazole (mCl_2DICz)

1 (6.35 g, 10 mmol), CuI (381 mg, 2mmol), hexamethylenetetramine (421 mg, 3 mmol), Cs_2CO_3 (13.02 g, 40 mmol) and 40 mL o-DCB were sequentially added to a 100 mL three-necked flask. The mixture was refluxed under nitrogen atmosphere overnight. After cooling to RT, yellow solid precipitate was collected by filtration. The solid was washed with saturated NH_4Cl solution, H_2O, MeOH and CH_2Cl_2. The obtained product (4.56 g, 96.3%) was directly subjected to the next step without further purification.

3,12-Dimesityldibenzo[2,3:5,6]pyrrolizino[1,7-bc]indolo[1,2,3-lm]carbazole ($mMes_2DICz$)

mCl_2DICz (2.37 g, 5 mmol), 2,4,6-trimethylbenzeneboronic acid (2.46 g, 15 mmol), Pd_2dba_3(114 mg, 0.125 mmol), Xphos (119 mg, 0.25 mmol), Cs_2CO_3 (6.51 g, 20 mmol) and Xylene/DMF (2: 1, 30 mL) were sequentially added to a 100 mL three-necked flask. The mixture was refluxed under nitrogen atmosphere overnight. After cooling to RT, the mixture was extracted with CH_2Cl_2, dried over anhydrous Na_2SO_4, and concentrated by rotary evaporation. The crude product was purified by column chromatography on silica gel using dichloromethane as eluent to afford **$mMes_2DICz$** (2.84 g, 88.8%) as yellow powder. ^{1}H NMR (500 MHz, Chloroform-*d*) δ 8.44 (d, *J* = 7.8 Hz, 2H), 8.39 (d, *J* = 7.6 Hz, 2H), 7.86 – 7.78 (m, 4H), 7.56 – 7.50 (m, 2H), 7.45 (t, *J* = 7.5 Hz, 2H), 7.29 (dd, *J* = 7.9, 1.4 Hz, 2H), 7.09 (s, 4H), 2.43 (s, 6H), 2.23 (s, 12H). ^{13}C NMR (126 MHz, Chloroform-*d*) δ 141.87, 139.85, 139.23, 138.91, 138.41, 137.05, 136.34, 128.94, 128.24, 127.57, 126.47, 124.57, 124.26, 123.01, 121.59, 113.13, 112.28, 111.89, 111.76, 21.13, 20.99. MALDI-TOF-MS: $C_{48}H_{36}N_2$: 640.29 Found: 640.57. Anal Calcd for $C_{48}H_{36}N_2$ (%): C, 89.97; H, 5.66; N, 4.37 Found: C, 90.04; H, 5.60; N, 4.36.

3,12-Bis(3,5-di-tert-butylphenyl)dibenzo[2,3:5,6]pyrrolizino[1,7-bc]indolo[1,2,3-lm]carbazole (mtPh$_2$DICz)

mtPh$_2$DICz was obtained by a method the same as that for **mMes$_2$DICz**. Yellow powder, yield: 2.52g, 64.5%. ^{1}H NMR (400 MHz, Chloroform-*d*) δ 8.21 (s, 2H), 8.04 (d, *J* = 7.7 Hz, 2H), 7.81 – 7.62 (m, 10H), 7.58 (t, *J* = 1.8 Hz, 2H), 7.48 (t, *J* = 7.7 Hz, 2H), 7.32 (t, *J* = 7.5 Hz, 2H), 1.55 (s, 36H). ^{13}C NMR (101 MHz, Chloroform-*d*) δ 151.27, 141.19, 141.15, 138.02, 137.06, 135.60, 128.89, 128.60, 125.97, 125.39, 124.16, 122.88, 121.89, 121.28, 121.07, 111.93, 111.83, 111.24, 111.18, 35.18, 31.75. MALDI-TOF-MS: $C_{58}H_{56}N_2$: 780.44 Found: 780.65. Anal Calcd for $C_{58}H_{56}N_2$ (%): C, 89.19; H, 7.23; N, 3.59 Found: C, 89.28; H, 7.19; N, 3.53.

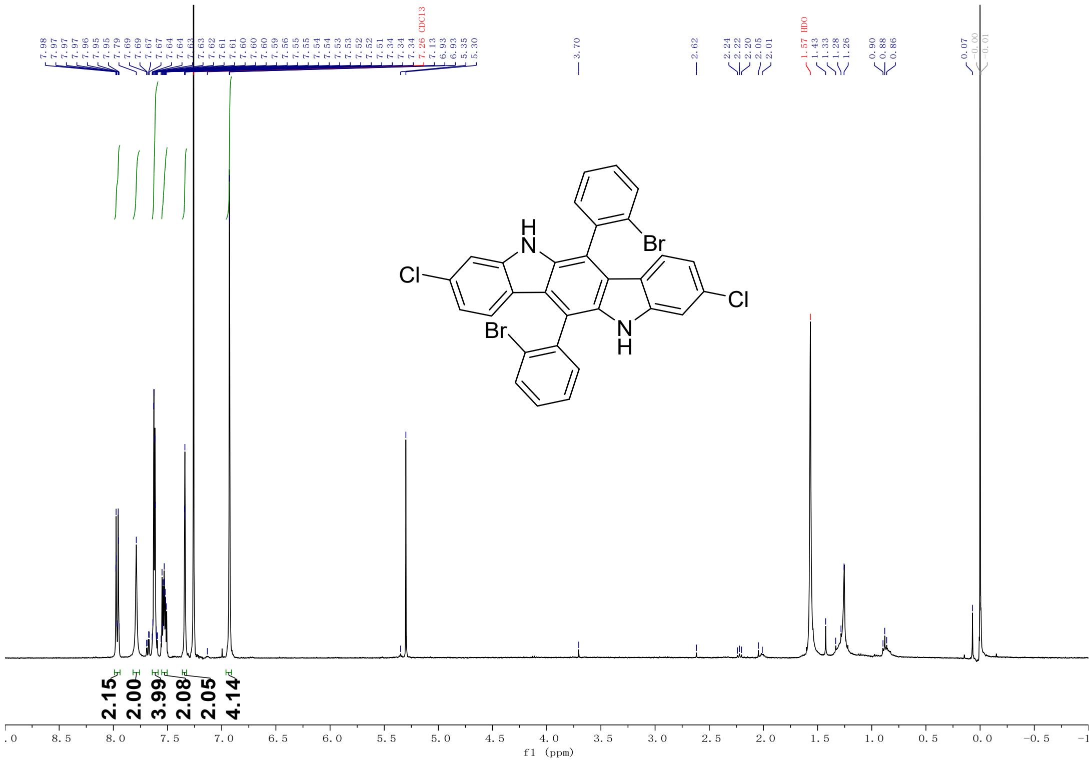

Figure S12. ^{1}H NMR spectra of **1**.

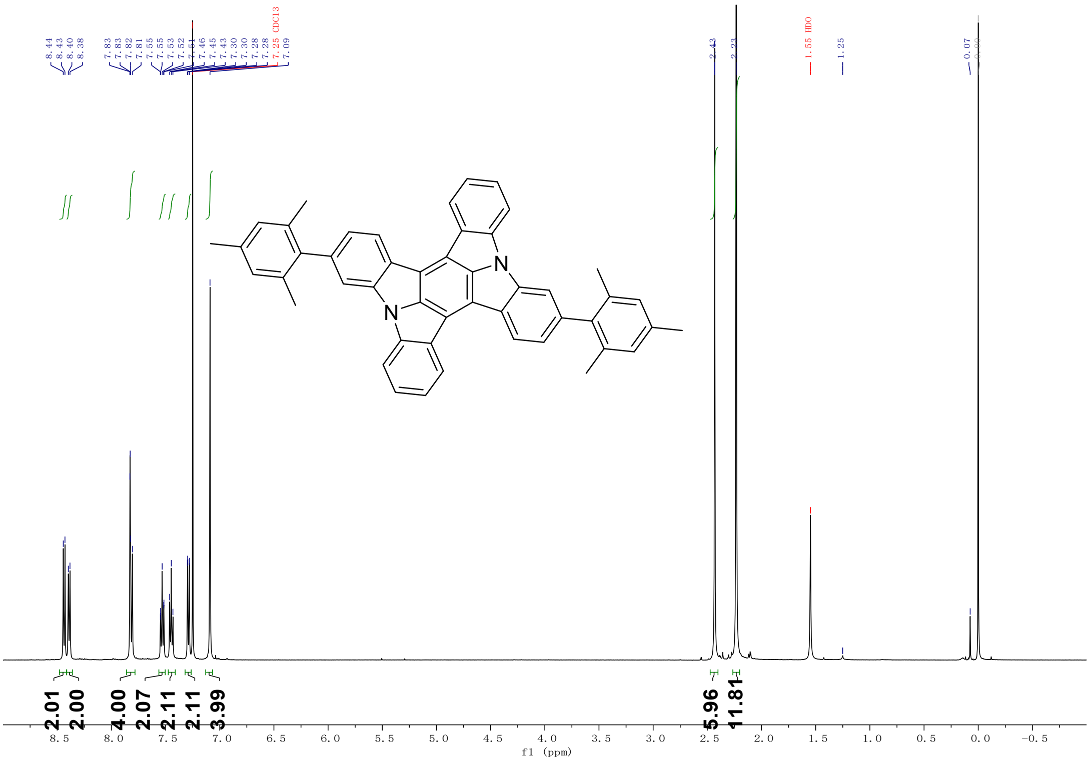

Figure S13. ^{1}H NMR spectra of mMes$_2$DICz.

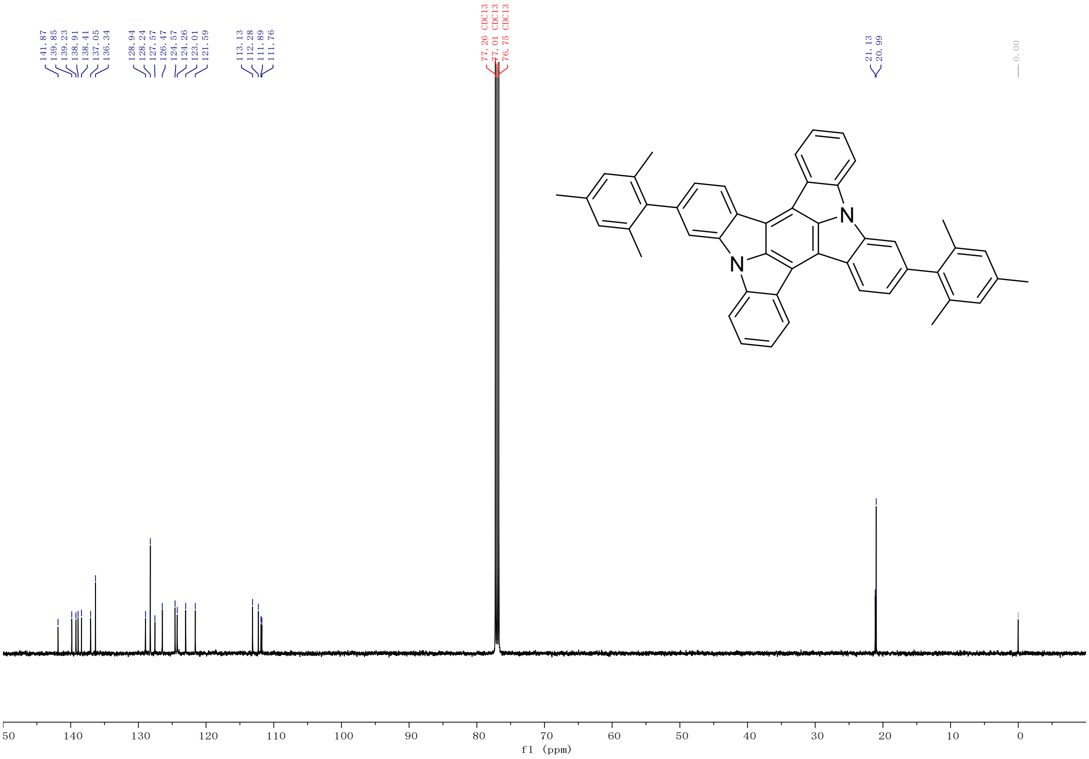

Figure S14. ^{13}C NMR spectra of mMes$_2$DICz.

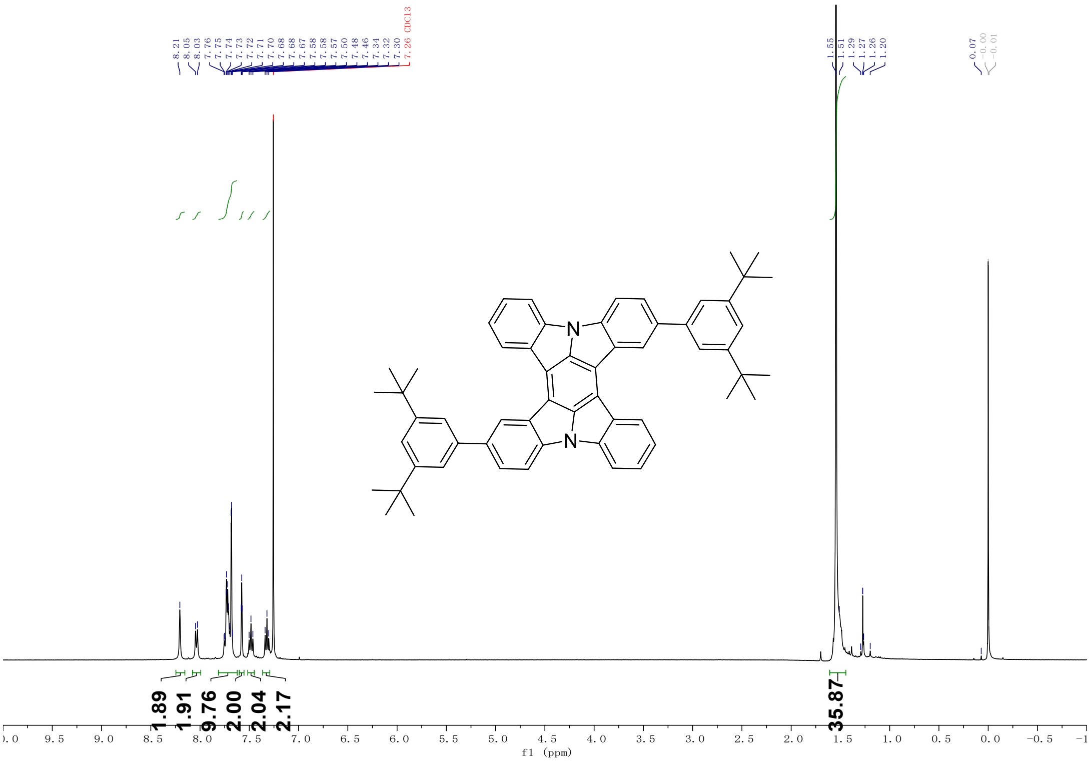

Figure S15. ^{1}H NMR spectra of mtPh$_2$DICz.

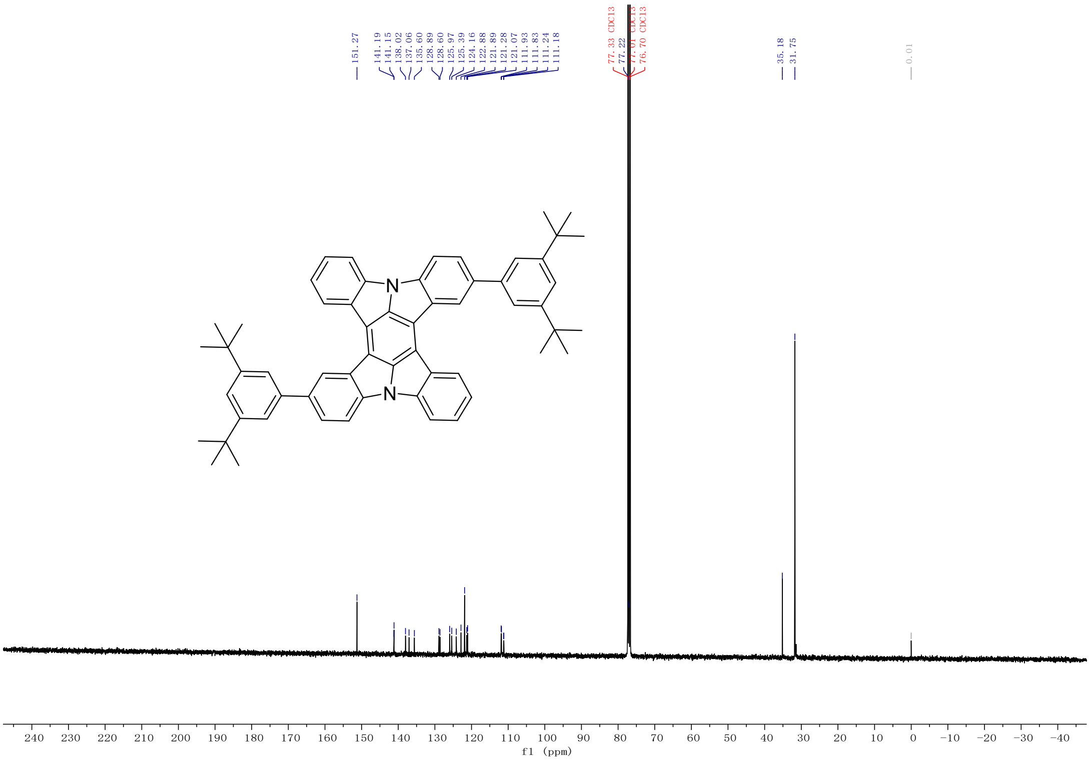

Figure S16. ^{13}C NMR spectra of mtPh$_2$DICz.

2.3 Photoluminescence (PL) measurements:

UV-VIS absorption was measured using a Shimadzu UV2600 UV/VIS spectrophotometer. The photoluminescence (PL) spectra and quantum yield of the samples were measured using a QM-40 spectrofluorometer (PTI, Horiba) equipped with a 150 W xenon lamp and an integrating sphere. The transient decay spectra were measured by the TCSPC technique, using a Horiba DeltaFlex modular. Lifetime measurement system equipped with a diode laser (λ=371 nm, pulse width ≈50 ps, repetition rate =20.00 kHz). The fluorescence decay curves were analyzed using the deconvolution software.

2.4 Electrochemical measurements:

Cyclic voltammetry was performed using a CHI 600E electrochemical analyzer in a gas-tight three-electrode cell at room temperature. A glassy carbon working electrode (Φ = 5.0 mm), a platinum wire auxiliary electrode, and an Ag/Ag^+ reference electrodes (0.1 M AgNO3, 0.1 M tetrabutylammonium hexafluorophosphate in acetonitrile) were used. The oxidation and reduction processes were measured by scanning the potential at a scan rate of 100 mV/s in CH2Cl2 and DMF, respectively, with 0.1 M tetrabutylammonium hexafluorophosphate (TBAP) as supporting electrolyte. The solutions were degassed by purging with N2 gas for approximately 3 minutes before the measurement. The ferrocene couple Fc^+/Fc was selected as the external reference.

2.5 Quantum chemical calculations:

All calculations were performed using the Gaussian 16 program package.[11] The ground state geometries were optimized via DFT calculations at the B3LYP/6-31g(d,p) level in vacuum. Frequency analysis was used to confirm that the structures are at the global minimum point of the potential surfaces. Based on the optimized ground state, the geometries of S1 state were optimized via TDDFT calculations at the B3LYP-D3BJ/6-31g(d,p) level in toluene.

2.6 Device fabrication and measurements:

The inorganic, organic and metal layers were thermally evaporated onto the substrates in an inert chamber under a pressure of 2×10^{-4} Pa. The active area of the devices is 9 mm^2. The deposition rates were 0.1 Å/s for Li_2CO_3 layer, 1−2 Å/s for organic layers, and 4 Å/s for Al layer. After fabrication, the devices were immediately encapsulated using glass cover slips and epoxy glue in a nitrogen-filled glove box (O2 < 0.1 ppm, H2O < 0.1 ppm). The luminance-current density-voltage characteristics and operational lifetimes for the devices were measured in ambient air with a Keithey 2400 Source meter and a Keithey 2000 Source multimeter equipped with a calibrated silicon photodiode. The electroluminescence spectra were recorded using a multichannel spectrometer (PMA12, Hamamatsu Photonics). Assuming Lambertian emission, the external quantum efficiency can be calculated from the luminance, current density, and EL spectrum.

3. References

[1] V. V. Patil, H. L. Lee, I. Kim, K. H. Lee, W. J. Chung, J. Kim, S. Park, H. Choi, W. J. Son, S. O. Jeon and J. Y. Lee, *Adv. Sci.*, 2021, **8**, e2101137.

[2] H. L. Lee, W. J. Chung and J. Y. Lee, *Small*, 2020, **16**, e1907569.

[3] V. V. Patil, J. Lim and J. Y. Lee, *ACS Appl. Mater. Interfaces*, 2021, **13**, 14440-14446.

[4] Z. Gao, Y. Liu, Z. Wang, F. Shen, H. Liu, G. Sun, L. Yao, Y. Lv, P. Lu and Y. Ma, *Chem. Eur. J.*, 2013, **19**, 2602-2605.

[5] C. M. Tonge, J. Zeng, Z. Zhao, B. Z. Tang and Z. M. Hudson, *J. Mater. Chem. C*, 2020, **8**, 5150-5155.

[6] W. Li, L. Yao, H. Liu, Z. Wang, S. Zhang, R. Xiao, H. Zhang, P. Lu, B. Yang and Y. Ma, *J. Mater. Chem. C*, 2014, **2**, 4733-4736.

[7] F. Qiu, D. Fang, J. Bai, T. Zhang, Y. Zhu, J. Miao, I. Murtaza, Z. Hu, C. Yan and H. Meng, *Dyes Pigm.*, 2020, **180**, 108458.

[8] S. Xiao, S.-T. Zhang, Y. Gao, X. Yang, H. Liu, W. Li and B. Yang, *Dyes Pigm.*, 2021, **193**, 109482.

[9] T. Sudyoadsuk, S. Petdee, C. Kaiyasuan, C. Chaiwai, P. Wongkaew, S. Namuangruk, P. Chasing and V. Promarak, *J. Mater. Chem. C*, 2021, **9**, 6251-6256.

[10] Y. Zheng, X. Zhu, Z. Ni, X. Wang, Z. Zhong, X. J. Feng, Z. Zhao and H. Lu, *Adv. Opt. Mater.*, 2021, **9**, 2100965.

[11] M. J. Frisch, G. W. Trucks, H. B. Schlegel, G. E. Scuseria, M. A. Robb, J. R. Cheeseman, G. Scalmani, V. Barone, G. A. Petersson, H. Nakatsuji, X. Li, M. Caricato, A. V. Marenich, J. Bloino, B. G. Janesko, R. Gomperts, B. Mennucci, H. P. Hratchian, J. V. Ortiz, A. F. Izmaylov, J. L. Sonnenberg, D. Williams-Young, F. Ding, F. Lipparini, F. Egidi, J. Goings, B. Peng, A. Petrone, T. Henderson, D. Ranasinghe, V. G. Zakrzewski, J. Gao, N. Rega, G. Zheng, W. Liang, M. Hada, M. Ehara, K. Toyota, R. Fukuda, J. Hasegawa, M. Ishida, T. Nakajima, Y. Honda, O. Kitao, H. Nakai, T. Vreven, K. Throssell, J. A. Montgomery, Jr., J. E. Peralta, F. Ogliaro, M. J. Bearpark, J. J. Heyd, E. N. Brothers, K. N. Kudin, V. N. Staroverov, T. A. Keith, R. Kobayashi, J. Normand, K. Raghavachari, A. P. Rendell, J. C. Burant, S. S. Iyengar, J. Tomasi, M. Cossi, J. M. Millam, M. Klene, C. Adamo, R. Cammi, J. W. Ochterski, R. L. Martin, K. Morokuma, O. Farkas, J. B. Foresman, and D. J. Fox, Gaussion 16, Revision A.03; Gaussian, Inc.: Wallingford CT, 2016.